Spinal cholinergic interneurons differentially control motoneuron excitability and alter the locomotor network operational range

Maria Bertuzzi and Konstantinos Ampatzis

Department of Neuroscience, Karolinska Institutet, 171 77 Stockholm, Sweden

Corresponding author: Konstantinos Ampatzis, Department of Neuroscience, Karolinska Institutet, SE-171 77 Stockholm, Sweden.

Tel: +46 8 524 87399, Fax: +46 8 349544, E-mail: Konstantinos.Ampatzis@ki.se

Summary

While cholinergic neuromodulation is important for locomotor circuit operation, the specific neuronal mechanisms that acetylcholine employs to regulate and fine-tune the speed of locomotion are largely unknown. Here, we show that cholinergic interneurons are present in the zebrafish spinal cord and differentially control the excitability of distinct classes of motoneurons (slow, intermediate and fast) in a muscarinic dependent manner. Moreover, we reveal that m2-type muscarinic acetylcholine receptors (mAChRs) are present in fast and intermediate motoneurons, but not in the slow motoneurons, and that their activation decreases neuronal firing. We also provide evidence that this configuration of motoneuron muscarinic receptors serves as the main intrinsic plasticity mechanism to alter the operational range of motoneuron modules. These unexpected findings provide new insights into the functional flexibility of motoneurons and how they execute locomotion at different speeds.

Introduction

Neural networks in the spinal cord are responsible for the generation and execution of movements (Goulding, 2009; Grillner, 2003; Grillner and Jessell, 2009; Kiehn, 2006). These spinal cord networks are organized in distinct functional microcircuit modules (Ampatzis et al., 2014; Bagnall and McLean, 2014) with defined operational ranges, whose sequential activation increases the speed of locomotion (Ampatzis et al., 2014). The activity of the spinal neuronal microcircuits is regulated by a range of neuromodulatory systems (Miles and Sillar, 2011) that permit motoneurons to adjust their final motor output. One such prominent neuromodulatory system is the cholinergic system (Miles et al., 2007; Zagoraiou et al., 2009). In rodents, cholinergic neuromodulation increases motoneuron excitability (Miles et al., 2007; Deardorff et al., 2014) in a task-dependent manner (Zagoraiou et al., 2009), which is exclusively mediated by cholinergic V0c interneurons (Zagoraiou et al., 2009). Whether cholinergic interneurons are present in the zebrafish spinal cord, and how they regulate the activity of the distinct motoneuron modules (slow, intermediate and fast) during locomotion is, however, unknown.

In mammals, acetylcholine release increases motoneuron excitability (Chevallier et al., 2006; Hornby et al., 2002; Ireland et al., 2012; Miles et al., 2007). Although m2 type metabotropic muscarinic acetylcholine receptor (m2-mAChR) activation is reported to mediate mammalian motoneuron hyperexcitability (Deardorff et al., 2014; Miles et al., 2007; Zagoraiou et al., 2009), numerous studies also demonstrate m2-mAChR-mediated inhibitory actions, in several neuronal populations (Brown, 2010; Felder, 1995; Hosey, 1992), including motoneurons (Kurihara et al., 1993). Moreover, m2-mAChRs are found to be predominantly expressed in large motoneurons (Welton et al., 1999). This suggests that only a subset of motoneurons are sensitive to cholinergic modulation via the m2-mAChRs. In order to resolve the question of whether m2 receptors are present in all motoneuron pools (slow, intermediate and fast), and

59 determine how activation of the m2-mAChRs influences the motoneuron functionality, we used
60 the accessible neuro-muscular configuration of the adult zebrafish (Ampatzis et al., 2013).

61 Using a combination of anatomical, electrophysiological, pharmacological, *ex vivo* and *in vivo*
62 behavioral approaches in adult zebrafish, we uncover a previously unidentified population of
63 spinal cord cholinergic interneurons that is analogous to mammalian V0c interneurons.
64 Furthermore, we provide the first functional evidence that cholinergic modulation acts as a
65 plasticity mechanism to differentially regulate the excitability and operational range of separate
66 motoneuron modules through activation of distinct mAChR subtypes.

67 **Results**

68 **Zebrafish spinal cholinergic system organization**

69 We first examined the distribution pattern of cholinergic terminals ($VAChT^+$) in the adult
70 zebrafish spinal cord. Multiple cholinergic terminals were detected in the dorsal horn, neuropil
71 and motor column (Figure 1A). Using the accessible neuro-muscular configuration of the adult
72 zebrafish, we dissected distinct functional motoneuron pools (Ampatzis et al., 2013). All
73 retrogradely traced secondary motoneuron types (slow, intermediate and fast) received
74 abundant cholinergic innervation (Figure 1B). To determine whether this innervation differs
75 among functionally different pools of secondary motoneurons, we analyzed the number of
76 cholinergic terminals ($VAChT^+$) in close proximity to motoneuron cell bodies (see Materials
77 and Methods). Fast motoneurons receive a significantly higher number of putative cholinergic
78 inputs than the intermediate and slow motoneurons (One-way ANOVA, $F_{2,64} = 16.69$, $p <$
79 0.0001, n = 67 neurons; Figure 1C). Furthermore, our analysis showed that these cholinergic
80 synapses on motoneurons do not display the typical morphology of the mammalian "c-boutons"
81 (Zagoraiou et al., 2009; Herron and Miles, 2012; Skup et al., 2012; Deardorff et al., 2014). To
82 investigate the origin of this input, we retrogradely labeled the brain neurons descending to

spinal cord (fluorescent Dextran tracer; see Material and Methods) and subsequently immunolabeled cholinergic neurons (Choline Acetyltransferase (ChAT) immunoreactivity; n = 8 brains). Our analysis revealed that none of these neurons were cholinergic as shown by the co-localization experiments (Supplementary file 1A-H). Moreover, few retrogradely labeled neurons in the initial part of the spinal cord were found to be cholinergic ($ChAT^{+}$) (Supplementary file 1I).

Having established that spinal cord cholinergic innervation is not provided by brain descending neurons, we hypothesized that spinal cord cholinergic interneurons account for the strong cholinergic input to motoneurons. This hypothesis is supported by the morphology of zebrafish motoneurons, which lack axonal collaterals (Ampatzis et al., 2013), that are recurrent axons that branch off from the main axon. In mammals, motoneuron collaterals form synaptic contacts with the Renshaw cells and other motoneurons (Eccles et al., 1954; Cullheim et al., 1977). Renshaw cells have not been reported in the zebrafish spinal circuits, and zebrafish motoneuron-motoneuron communication is meditated through dendro-dendritic electrical gap junctions (Song et al., 2016). We tested our hypothesis using two complementary approaches. First, we employed the *Islet1:GFP* zebrafish line, in which all motoneurons express green fluorescent protein (GFP; Uemura et al., 2005) and labeled both motoneurons and cholinergic interneurons through ChAT immunoreactivity (Figure 1D). We identified a significant fraction (38.17 ± 2.523%, Figure 1E), of small to medium size non-motoneuron cholinergic neurons ($ChAT^{+}Islet1^{-}$, 40.13 ± 1.038 μm^2; Figure 1F), which were distributed throughout the motor column (Figure 1G). In comparison, identified motoneurons were larger ($ChAT^{+}Islet1^{+}$, 69.04 ± 4.729 μm^2; Figure 1F). To further confirm that all the $ChAT^{+}Islet1^{-}$ are indeed interneurons and not motoneurons which had lost the GFP expression in the *Islet1* line, we injected a retrograde tracer into zebrafish spinal cord ventral roots (see Material and Methods; Figure 1H) and combined it with ChAT immunoreactivity (Figure 1I). Given that all zebrafish motoneuron

axons exiting from the same ventral root correspond to the spinal hemisegment, this approach enabled us to reveal all the spinal motoneurons (axial and fin; Figure 1H). We observed that 37.37 ± 3.75% (Figure 1J) of the cholinergic neurons are not motoneurons, similar to findings in the *Islet1* zebrafish transgenic line.

Finally, to assess whether spinal cholinergic interneurons innervate targets located in rostral or caudal spinal cord segments, we identified cholinergic interneurons (into segment 15) as ascending or descending, after injection of a retrograde tracer (dextran) into segments 12 or 18, respectively, in an *Islet1:GFP* line (n=14 zebrafish; Figure 1J,K). 24h after the tracer injection we processed the tissue for ChAT immunostaining. We observed that 7.56% of $ChAT^{+}Islet1^{-}$ neurons were labelled as descending neurons (Supplementary file 1J, L, M), and 13.22% of $ChAT^{+}Islet1^{-}$ neurons were determined as ascending neurons (Supplementary file 1K-M), indicating that 20.78% of the cholinergic interneurons project to other spinal cord segments. The significant difference between the soma size of the ascending and descending cholinergic interneurons suggest that they form two non-overlapping neuronal subpopulations (Supplementary file 1N). Overall, our data suggest that zebrafish spinal motoneurons receive unevenly distributed cholinergic input from a local spinal source, represented by cholinergic interneurons.

V0c interneurons are present in zebrafish spinal cord

Most (~75%) ChAT interneurons ($ChAT^{+}Islet1^{-}$) were found in the dorsal part of the motor column close to the central canal (Figure 1G), where the mammalian V0c interneurons are also positioned (Zagoraiou et al., 2009). Previously, it was assumed that V0c interneurons do not exist in zebrafish (Satou et al., 2012). To test if the observed zebrafish spinal cholinergic interneurons correspond to the mammalian V0c interneurons, we combined *in situ* hybridization for *Pitx2,* a paired-like homeodomain transcription factor that marks V0c

interneurons in mammals (Figure 2A; Zagoraiou et al. 2009), with ChAT immunolabeling (Figure 2B). Our analysis revealed that 28.36 ± 1.83 % of the ChAT neurons were also *Pitx2* positive (*Pitx2*$^{+}$; Figure 2C). Although the *Pitx2*$^{+}$ neurons were distributed throughout the motor column, ~80% were located around the central canal (Figure 2D), suggesting that an equivalent of mammalian V0c interneurons do exist in zebrafish. Moreover, we performed whole cell patch clamp recordings from several unidentified neurons located around the central canal. We found that 3 neurons out of 20 were cholinergic and not motoneurons, and they displayed intrinsic electrical properties (i.e. prominent after-hyperpolarization, rheobase, lack of neuronal sag) comparable to the mammalian V0c interneurons (Zagoraiou et al. 2009; Figure 2E). Although these interneurons do not receive rhythmic synaptic inputs during locomotion, they receive strong synaptic potentials at speeds < 6 Hz (paired t test, $t = 5.133$ $df = 40$, $p < 0.0001$, $n = 3$ neurons; Figure 2F).

It was apparent that the cholinergic interneurons are not active during regular swimming (< 6Hz), so we next assessed when these cholinergic interneurons operate, contributing to locomotor network functionality. To address this issue, we subjected adult zebrafish to forced fast swimming test (80% of the critical speed (Ucrit), see Material and Methods) for 2 h, followed by functional anatomical analysis of *c-fos* expression as an index of neuronal activity. Analysis of *c-fos* intensity in all ChAT^{+}Islet1^{-} neurons revealed that more neurons are active (54%) during fast swimming, compared to the control, as indicated by a significant increase in *c-fos* expression (unpaired t test, $t = 2.89$ $df = 60$, $p = 0.0054$; Figure 2G-J). Our observations are in agreement with previous analysis performed in the cat spinal cord, which showed that cholinergic neurons close to the central canal were functionally active during prolonged fictive locomotion (Huang et al., 2000). Collectively, our results demonstrate that the vast majority of the zebrafish cholinergic interneurons (80%) are analogues to mammalian V0c interneurons and their activity is related to prolonged fast locomotion.

Muscarinic receptors differentially alter motoneuron excitability

In mammals, acetylcholine increases the excitability of spinal motoneurons through the activation of muscarinic receptors (Miles et al., 2007). To investigate whether zebrafish motoneuron excitability is responsive to activation of mAChRs we obtained whole cell current clamp recordings from different classes (slow, intermediate and fast) of axial secondary motoneurons. Since the fast and intermediate motoneurons discharge single action potentials (APs), whereas slow motoneurons fire in bursts of APs (Gabriel et al., 2011; Ampatzis et al., 2013), the excitability of motoneurons was assessed by examining their response (number of single APs or number of bursts) to steps of supra-threshold depolarizing current pulses (500 ms, increments of 10% from rheobase), before and after the application of muscarine, a non-selective mAChR agonist. In the presence of muscarine (15 μM), the firing rate of both slow (one-way ANOVA repeated measures, $F_{1.319, 5.277} = 16$, $p = 0.021$, n = 5 out of 5) and intermediate (one-way ANOVA repeated measures, $F_{1.269, 6.344} = 24.36$, $p = 0.0079$, n = 6 out of 6 neurons) motoneurons substantially increased (Figure 3A-C, F). This was accompanied by an increase of the input resistance (slow MNs: one-way ANOVA repeated measures, $F_{1.059, 4.237} = 13.34$, $p = 0.0227$; intermediate MNs: one-way ANOVA repeated measures, $F_{1.493, 7.466} = 12.64$, $p = 0.0258$; Figure 3E) and changes in other intrinsic biophysical properties (Supplementary file 2), without significantly altering the resting membrane potential (Figure 3D). In contrast, the fast motoneurons showed a decrease in excitability, resulting in fewer action potentials (one-way ANOVA repeated measures, $F_{1.986, 15.89} = 38.05$, $p < 0.0001$, n = 9 out of 9 neurons; Figure 3A,B,F) associated with a significant decrease of the input resistance (one-way ANOVA repeated measures, $F_{1.12, 8.958} = 4.462$, $p = 0.0141$, Figure 3E). Moreover, alterations of the electrical properties of fast motoneurons were similar to those observed in the intermediate motoneurons (Supplementary file 2). The observed changes in intrinsic biophysical properties of the motoneurons are consistent with previously reported alterations of mammalian

182 motoneurons in response to muscarine (Ireland et al., 2012).

183

184 **Motoneurons possess different muscarinic receptor subtypes**

185 We speculated that the differential motoneuron excitability we observed might arise from the
186 presence of different mAChR subtypes in the motoneurons. To test if m2-mAChRs alone
187 mediate the changes in motoneuron excitability, we applied a mixture of muscarine (15 μM)
188 and methoctramine (10 μM), a selective m2-mAChR antagonist (Hulme et al., 1990). We
189 recorded an increase in excitability of fast (paired t test, $t = 3.641$, $p = 0.0219$, $n = 5$ out of 5
190 neurons; Figure 4A-C), intermediate (paired t test, $t = 4.323$, $p = 0.0228$, $n = 4$ out of 4 neurons)
191 and slow (paired t test, $t = 4.00$, $p = 0.0161$, $n = 3$ out of 3 neurons) motoneurons (Figure 4A-
192 C). To assess whether m2-mAChRs are present in all classes of motoneurons, we applied
193 oxotremorine-M (Oxo-M; 20 μM), an m2-mAChR preferential agonist (Murakami et al., 1996).
194 In response, the fast (paired t test, $t = 10.00$, $p = 0.0005$, $n = 5$ out of 5 neurons) and intermediate
195 (paired t test, $t = 6.668$, $p = 0.0026$, $n = 5$ out of 5 neurons) motoneurons exhibited reduced
196 firing (Figure 4D-F), whereas, slow motoneuron firing was unaffected (paired t test, $t = 1.00$, p
197 $= 0.391$, $n = 4$ out of 4 neurons; Figure 4D-F), suggesting that they do not express the m2-
198 mAChR subtype. Moreover, we confirmed the presence of m2-mAChRs in motoneurons
199 anatomically. Immunoreactivity for the m2-mAChRs was strong in fast motoneurons and
200 modest in intermediate motoneurons (One-way ANOVA, $F_{2,35} = 51.32$, $p < 0.0001$, $n = 38$
201 neurons; Figure 4G, H). In contrast, slow motoneurons were weakly labeled for the m2-
202 mAChR, supporting previous reports (Welton et al., 1999; Figure 4G, H). These results indicate
203 that multiple mAChR subtypes are expressed in a motoneuron type-dependent manner, which
204 functions to differentially mediate the actions of acetylcholine.

205

206 **Activation of motoneuron muscarinic receptors controls fast locomotion**

Given that motoneuron excitability can retrogradely influence the upstream locomotor network function (presynaptic release, generation of action potentials, swimming duration and frequency) through gap junctions (Song et al., 2016), we tested the functional significance of motoneuron mAChR activation during locomotion. For this, we used the adult zebrafish *ex vivo* preparation (Ampatzis et al., 2013; Ampatzis et al., 2014; Gabriel et al., 2011; Song et al., 2016). Bath application of muscarine facilitated fictive locomotor activity and increased the highest reached swimming frequency by 26.8 ± 5.8 % (paired t test, $t = 6.675$, $p < 0.0001$, $n = 12$; Figure 5A-B). It should be noted that the amplitude of the swimming membrane potential oscillations during locomotion is related to swimming frequency (Gabriel et al., 2011). In the presence of muscarine, the correlation between oscillation amplitude and frequency was decreased in the fast motoneurons (Figure 5C) and enhanced in the intermediate motoneurons that were recruited above 7 Hz (Figure 5D). Furthermore, we investigated the number of APs in the slow and intermediate motoneurons during ongoing fictive locomotion at 5 Hz (Figure 5E). At this swimming speed, we found that only the intermediate motoneurons discharge more action potentials in the presence of muscarine, compared to controls (paired t test, $t = 3.43$, $p = 0.0018$; Figure 5E). Overall, our findings demonstrate that activation of spinal muscarinic receptors facilitates the recruitment of the intermediate motoneuron-interneuron module while hindering the recruitment of the fast locomotor module, as seen through the motoneuron activation.

Finally, we sought to better understand the *in vivo* behavioral functions of the activation of mAChRs. Therefore, we subjected zebrafish to a critical speed test (Supplementary file 3; see Supplemental Experimental Procedures). Critical speed (U_{crit}) is a measure of the highest sustainable swimming speed that a fish can reach (Brett, 1964). Intraperitoneal administration of muscarine (50 µM, 525 ng/g BW; Supplementary file 3A) significantly reduced the highest sustainable swimming speed (unpaired t test, $t = 2.65$, $p = 0.014$, $n = 23$ zebrafish; Figure 5F).

In contrast, methoctramine treated animals (40 μM, 2.2mg/g BW; Supplementary file 3) increased the uppermost locomotor speed (unpaired t test, $t = 2.12$, $p = 0.047$, $n = 20$ zebrafish; Figure 5G). Similarly, exogenous activation of all muscarinic receptors except the m2-mAChRs, achieved by co-administration of muscarine (50 μM) and methoctramine (40 μM), increased the maximum locomotor speed obtained (unpaired t test, $t = 2.156$, $p = 0.046$, $n = 18$ zebrafish; Figure 5H).

To test the effect of our pharmacological treatments on locomotion under normal conditions, animals were subjected to an open field test (Supplementary file 3, see Material and Methods). We observed that similar treatment did not affect the regular locomotor behavior (distance traveled, average velocity and maximum velocity; Figure 5I-K), suggesting that the differences in critical speed observed here are due to the effect on the spinal locomotor circuit. These data show that stimulation of m2-mAChRs causes a reduction in the maximum swimming speed to 76.5 ± 6.7 % of the of the U_{crit}, corresponding to the zebrafish optimum speed (Palstra et al., 2010), where swimming relies only on the activity of the slow and intermediate neuro-muscular system, and not on the fast. Our analysis cannot rule out the possibility of an additional direct effect of mAChR activation in the premotor neurons, however, as any alteration in motoneuron excitability will retrogradely affect the excitability and pre-synaptic release of glutamate from V2a interneurons (Song et al., 2016), which will influence premotor network functionality. Taken together, our results suggest that cholinergic modulation acts both on motoneurons and the premotor network to modify the speed of locomotion mainly through the engagement of the fast motoneuron-interneuron module.

Discussion

Our findings suggest that motoneurons receive cholinergic input exclusively from spinal interneurons, with the vast majority of them being analogous to mammalian V0c interneurons.

Acetylcholine shifts motoneuron excitability through the parallel activation of different mAChRs subtypes (Figure 6A). Moreover, activation of this pathway selectively alters the operational range of different motoneuron modules during locomotion (Figure 6B). Overall, this work provides novel insights into how intraspinal acetylcholine release can modify the functionality of the spinal circuitry, which requires synaptic specificity and temporal precision to generate locomotion at different speeds (Ampatzis et al., 2013; Ampatzis et al., 2014).

One of our major findings is establishing the existence of cholinergic interneurons in the zebrafish spinal cord and identifying them as the exclusive source of the cholinergic spinal input. Although earlier studies showed the existence of cholinergic interneurons in several vertebrate species (Thiriet et al., 1992; Anadón et al., 2000; González et al., 2002; Miles et al., 2007; Quinlan and Buchanan, 2008; Zagoraiou et al., 2009), and moreover, the zebrafish cholinergic system is well characterized (Clemente et al., 2004; Mueller et al., 2004), the presence of zebrafish spinal cord cholinergic interneurons has not been previously reported. While a number of $Chat^{+}Islet1^{-}$ neurons were identified earlier (Stil and Drapeau, 2016), it has been proposed that these small cholinergic neurons correspond to motoneurons, rather than the ones that innervate the axial muscles (Muller et al., 2004). Previous attempts to localize *Pitx2* expression with *Dbx1* in order to reveal the existence of V0c interneurons in zebrafish spinal cord were ineffective (Satou et al., 2012). In the current study we used a different approach, by combining *Pitx2* expression with ChAT immunostaining, to achieve this goal. We revealed that most cholinergic interneurons share comparable anatomical distribution, molecular identity and electrical properties with mammalian V0c interneurons. Our analysis cannot rule out the possibility that more cholinergic interneuron subtypes are present in zebrafish spinal cord. However, most of zebrafish cholinergic interneurons (~80%) express *Pitx2*, thus we considered them to be similar to mammalian V0c interneurons. Since V0c interneurons have been shown

281 to be the exclusive source of cholinergic c-bouton input to mammalian motoneurons (Zagoraiou
282 et al. 2009), our data directly implicate the activity of these cholinergic interneurons in the
283 cholinergic modulation of motoneurons in the zebrafish.
284 The overall activation of the muscarinic receptors has been shown to increase motoneuron
285 excitability (Alaburda et al., 2002; Chevallier et al., 2006; Hornby et al., 2002; Ireland et al.,
286 2012; Miles et al., 2007) via activation of the m2-mAChR subtype (Miles et al., 2007). On the
287 other hand, numerous studies have shown that activity of the m2-mAChRs is associated with
288 inhibitory actions in the nervous system (Brown, 2010; Felder, 1995; Hosey, 1992; Kurihara et
289 al., 1993). Our findings challenge previous conclusions that activation of motoneuron m2-
290 mAChR is primarily required to increase motoneuron excitability. By pharmacologically
291 manipulating the m2-mAChRs in different motoneuron pools, we found that m2-mAChR
292 activation reduces motoneuron excitability and other receptor subtypes can account for the
293 observed rise in motoneuron firing. In line with this idea, various subtypes of mAChRs have
294 been characterized in the spinal cord neurons (Brown, 2010; Höglund and Baghdoyan, 1997;
295 Zhang et al., 2005; Jordan et al., 2014) and it is also well documented that many nerve cells
296 contain more than one subtype of muscarinic receptor (Finkel et al., 2014; Hassall et al. 1993;
297 Jordan et al., 2014). The exact muscarinic receptor subtype responsible for the elevated
298 excitability of adult zebrafish motoneurons remains to be identified. However, it has been
299 suggested that the excitatory effects of muscarinic agonists on neonatal rat motoneurons are
300 mediated through the m3-mAChRs (Kurihara et al., 1993). In support of our observations,
301 Jordan et al. (2014) recently demonstrated that m2-mAChRs and m3-mAChRs are both
302 involved in the cholinergic modulation of locomotion in mammals. They showed that
303 application of the m2-mAChR antagonist methoctramine, increased the locomotor rhythm,
304 whereas application of m3-mAChR antagonist reduced, and finally blocked, the locomotor
305 activity (Jordan et al., 2014). Our results show that different muscarinic receptor subtypes in

306 the membrane of motoneurons can play a unique role in the regulation of neural activity
307 involved in the control of locomotion.
308
309 Given the emerging evidence regarding the importance and functional repertoire of spinal
310 cholinergic input in the control of motor behaviors, it is not surprising that cholinergic synapses
311 have been implicated in spinal cord injury (Ichiyama et al., 2011; Skup et al., 2012; Jordan et
312 al., 2014) and motor disease (Herron and Miles, 2012; Pullen and Athanasiou, 2009; Saxena et
313 al., 2013). However, no causal link has yet been found between alterations in the number and
314 size of cholinergic synapses, acetylcholine release and muscarinic receptor activation.
315 Therefore, uncovering the mechanisms by which acetylcholine modifies the activity of spinal
316 neurons is of significant biological and medical interest. We find that methoctramine treated
317 animals are able to operate at higher swimming speeds and, in addition, activation of m2-
318 mAChRs reduces the excitability of the motoneurons, and potentially of other spinal cord
319 neurons, and their ability to produce the appropriate muscle force. In support of our findings,
320 Jordan et al., (2014) revealed that application of methoctramine increased the locomotor
321 frequency in mammals. Moreover, application of cholinergic receptor antagonists following
322 spinal cord injury was found to advance locomotor activity, suggesting that adaptive alterations
323 of the spinal cholinergic system obstruct the generation and execution of locomotion (Jordan et
324 al., 2014). In a mouse model of amyotrophic lateral sclerosis (ALS), methoctramine treatment
325 counteracts the loss of muscle force during the pre-symptomatic stages of the disease (Saxena
326 et al., 2013), and is likely to be mediated through the blocking of m2-mAChRs, increasing the
327 excitability of spinal neurons participating in the generation of movement. In conclusion, our
328 results provide a novel contribution to existing knowledge, and further understanding of the
329 causal relationship between activation of muscarinic receptors and locomotion, highlighting
330 their potential as targets for innovative therapeutic strategies.

A general question about the cholinergic control of locomotion is made addressable in our work: how does the muscarinic acetylcholine receptor configuration gate the execution of locomotor behavior at different speeds? It has been proposed that the cholinergic modulation of motoneurons is activity dependent (Zagoraiou et al., 2009). In favor of this idea, our work revealed that pharmacological manipulations of spinal circuit muscarinic receptors *ex vivo* and *in vivo* only affect the locomotor performance of zebrafish at higher swimming speeds, which are primarily associated with the engagement and function of the fast motoneuron-interneuron module. Thus, the mechanisms we identify here suggest an additional level of control during high-energy-demand locomotion, such as fast swimming.

Materials and Methods

Animals

All animals were raised and kept in a core facility at the Karolinska Institute according to established procedures. Adult zebrafish (*Danio rerio*; 8-10 weeks old; length, 17-19 mm; weight, 0.025-0.045 g) wild type (AB/Tübingen) and Tg(*Islet1:GFP*) lines where used in this study. All experimental protocols were approved by the local Animal Research Ethical Committee, Stockholm and were performed in accordance with EU guidelines.

Motoneuron and descending/ascending neuron labeling

Zebrafish (n = 30) of either sex were anaesthetized in 0.03% tricaine methane sulfonate (MS-222, Sigma-Aldrich). Retrograde labeling of axial motoneurons was performed using dye injections with tetramethylrhodamine-dextran (3000 MW; ThermoFisher, D3307) in specific muscle fiber types (slow, intermediate or fast). In addition, retrograde labeling of all motoneurons was performed using similar procedure to spinal cord ventral roots. To label the

355 neurons descending from the brain to the spinal cord the tracer was injected using dye-soaked
356 pins in the spinal cord at approximately the level of the 6-8th vertebra. Finally, for the
357 investigation of descending and ascending cholinergic interneurons the tracer was injected in
358 the spinal segment 18 (n = 7 zebrafish) or 12 (n = 7 zebrafish) respectively. Afterwards all the
359 animals were kept for at least 24h to allow the retrograde transport of the tracer. We evaluated
360 the number of $ChAT^{+}Istlet1^{-}$ ineterneurons that were positive to the tracer on segment 15 of the
361 adult zebrafish spinal cord.
362
363 **Immunohistochemistry**
364 All animals were deeply anesthetized with 0.1% MS-222. We then dissected the spinal cords
365 and/or the brains and fixed them in 4% paraformaldehyde (PFA) in phosphate buffer saline
366 (PBS) (0.01M; pH = 7.4) at 4°C for 2-14h. We performed immunolabelings in both whole
367 mount and cryosections. For cryosections, the tissues were removed carefully and cryoprotected
368 overnight in 30% (w/v) sucrose in PBS at 4°C, embedded in OCT Cryomount (Histolab),
369 rapidly frozen in dry-ice-cooled isopentane (2-methylbutane; Sigma) at approximately –35°C,
370 and stored at –80°C until use. Transverse coronal plane cryosections (thickness 25 µm) of the
371 tissue were collected and processed for immunohistochemistry. The tissue was washed three
372 times for 5 min in PBS. Nonspecific protein binding sites were blocked with 4% normal donkey
373 serum with 1% bovine serum albumin (BSA; Sigma) and 0.5% Triton X-100 (Sigma) in PBS
374 for 30 min at room temperature (RT). Primary antibodies were diluted in 1% of blocking
375 solution and applied for 24-90 hours at 4 °C. For primary antibodies, we used goat anti-ChAT
376 (1:200; Millipore, AB144P, RRID: AB_2079751), rabbit anti-GFP (1:700; ThermoFisher
377 Scientific, A-11122, RRID: AB_221569), guinea pig anti-VAChT (1:1000; Millipore, AB1588,
378 RRID: AB_11214110), rabbit anti-cfos (1:200; Sigma, F7799) and rabbit anti-m2 mAChRs
379 (1:700-1:2000; Alomone, AMR-002, RRID: AB_2039995). After thorough buffer rinses the

tissues were then incubated with the appropriate secondary antibodies diluted 1:500 in 0.5% Triton X-100 (Sigma) in PBS overnight at 4 °C. We used Alexa Fluor–conjugated secondary antibodies anti-goat 488 (ThermoFisher Scientific, A11055, RRID: AB_142672), anti-goat 568 (ThermoFisher Scientific, A11057, RRID: AB_142581), anti-rabbit 488 (ThermoFisher Scientific, A21206, RRID: AB_141708) and anti-guinea pig 488 (ThermoFisher Scientific, A11073, RRID: AB_142018). Finally, the tissues were thoroughly rinsed in PBS and cover-slipped with fluorescent hard medium (VectorLabs; H-1400).

In situ hybridization

Adult zebrafish wild type (AB/Tübingen) spinal cords were fixed, cryoprotected and cryosectioned (thickness of 12 μm) as described before (see *Immunohistochemistry* section). Coronal transverse section then processed for fluorescent *in situ* hybridization using the RNAscope Technology (Advance Cell Diagnostics), according to manufacturer's instructions. Target probe for zebrafish specific *Pitx2* gene (Advance Cell Diagnostics, 432161-C3) was used. After the detection of *Pitx2* mRNA, tissues were processed for ChAT immunodetection as described before (*Immunohistochemistry section*). To investigate how many of cholinergic neurons are *Pitx2*, 3 sections per animal (n = 4 zebrafish) corresponding to 12-14th spinal cord segments were analyzed.

***c-fos* functional anatomy**

Adult zebrafish (*Islet1:GFP*; n = 8) were used for c-fos experiments. Animals were subjected to forced swim test. We used two different experimental protocols to investigate the activity of cholinergic interneurons. Animals were subjected to prolonged swimming (2 h) at 80% of the critical speed (U_{crit}). Control animals were kept under regular tank swimming conditions. Immediately after the test all animals were fixed and processed for triple immunolabeling,

against *c-fos*, the ChAT and the GFP (see Supplemental Experimental Procedures, section Immunohistochemistry) in 25 μm thick cryosections. For the *c-fos* experiments, analysis was performed in neurons (n=62) from sections corresponding to segments 14-17. The intensity of the *c-fos* activity was evaluated in the obtained confocal pictures using ImageJ.

Microscopy and image analysis

Imaging was carried out in a laser scanning confocal microscope (LSM 510 Meta, Zeiss). Cholinergic inputs on different motoneuron types were counted on single plan confocal images. Counting was performed in non-overlapping fields of spinal cord sections, in spinal cord segments 14-17. We defined the putative cholinergic inputs as number of large (>0.5 μm of diameter) VAChT-positive putatively cholinergic synapses, apposing the somata of motoneurons. The evaluation included 10 slow, 27 intermediate and 30 fast positive motoneurons collected from 4 adult zebrafish spinal cords. For the quantification of m2-mAChRs, all images were captured at identical exposure times in order to ensure the same illumination level. The intensity of m2-mAChRs immunoreactivity was evaluated in the obtained confocal pictures using the ImageJ image analysis software. The relative position of the somata of the neurons within spinal cord, was calculated in whole mount preparations, using the lateral, dorsal, and ventral edges of spinal cord as well as the central canal as landmarks. Analysis of all spinal cord neurons was performed between segments 14-17. The relative position was calculated using ImageJ. Examination of the descending neurons was performed from a series of coronal brain section, throughout the brain, without discarding any section from the analysis. The nomenclature used for the brain areas of descending neurons was based on the topological zebrafish brain atlas (Wullimann et al., 1996). All figures and graphs were prepared with Adobe Photoshop and Adobe Illustrator (Adobe Systems Inc., San Jose, CA). All double-labeled images were converted to magenta-green immunofluoresence to make this work more accessible to the red-green color-blind readers.

Ex vivo preparation and electrophysiology

The dissection procedure has been described previously (Gabriel et al., 2011; Ampatzis et al., 2013; Ampatzis et al., 2014; Song et al., 2016). The preparations (n = 47) were then transferred to a recording chamber, placed lateral side up, and fixed with Vaseline. The chamber was continuously perfused with extracellular solution contained: 134 mM NaCl, 2.9 mM KCl, 2.1 mM $CaCl_2$, 1.2 mM $MgCl_2$, 10 mM HEPES, and 10 mM glucose, pH 7.8, adjusted with NaOH, and an osmolarity of 290 mOsm. All experiments were performed at an ambient temperature of 20–22°C. For whole-cell intracellular recordings, electrodes (resistance, 9–13 MΩ) were pulled from borosilicate glass (outer diameter, 1.5 mm; inner diameter, 0.87 mm; Hilgenberg) on a vertical puller (PC-10 model, Narishige) and filled with intracellular solution containing the following: 120 mM K-gluconate, 5 mM KCl, 10 mM HEPES, 4 mM Mg_2ATP, 0.3 mM Na_4GTP, 10 mM Na-phosphocreatine, pH 7.4, adjusted with KOH, and osmolarity of 275 mOsm. Dextran-labeled MNs were visualized using a fluorescence microscope (Axioskop FS Plus, Zeiss) equipped with IR-differential interference contrast optics and a CCD camera with frame grabber (Hamamatsu) and were then targeted specifically. Intracellular patch-clamp electrodes were advanced in the exposed portion of the spinal cord through the meninges using a motorized micromanipulator (Luigs & Neumann) while applying constant positive pressure. Intracellular signals were amplified with a MultiClamp 700B intracellular amplifier (Molecular Devices) and low-pass filtered at 10 kHz. In current-clamp recordings, no bias current was injected. Only motoneurons that had stable membrane potentials at or below –48 mV fired action potentials to suprathreshold depolarizations and showed minimal changes in series resistance (<5%) were included in this study. In some experiments neurons were passively filled with 0.25% neurobiotin tracer (Vector Labs) for post hoc analysis of their neurochemical identity. Spinal cords with neurobiotin-filled neurons were dissected out and transferred in 4% PFA solution at 4 °C for 3 h. The tissue was then washed extensively with PBS, and incubated

455 in streptavidin conjugated to Alexa Fluor 555 (1:500; Invitrogen, SP-1120) and were used for
456 detection of ChAT immunoreactivity following the protocol described above. The following
457 drugs were added to the physiological solution: non-selective muscarinic receptor agonist
458 muscarine (15 µM; Sigma, M104), m2-type selective muscarinic receptor antagonist
459 methoctramine (10 µM; Sigma, M105) and m2-type preferential muscarinic receptor agonist
460 oxotremorine-M (20 µM; Sigma, O100). All drugs were dissolved as stock solutions in distilled
461 water. For all the electrophysiological recordings data analysis was performed using Spike2
462 (version 7, Cambridge Electronic Design) or Clampfit (Molecular Devices) software. The
463 action potential voltage threshold of motoneurons was determined from the measured
464 membrane potential at which the *dV/dt* exceeded 10 mV/msec.
465
466 ***In vivo* swimming behavior**
467 The swimming ability of zebrafish was tested using the open field test and the critical speed
468 (U_{crit}) test. U_{crit} is a measure of the highest sustainable swimming speed achievable by a fish.
469 All zebrafish (n = 80) selected for the test displayed similar body length sizes and body weights.
470 Animals were first anaesthetized in 0.03% tricaine methane sulfonate (MS-222, Sigma-Aldrich)
471 in fish water and injected intraperitoneally (volume: 2 µl) with saline, muscarine (50µM; 525
472 ng / g body weight) or/and methoctramine (40 µM; 2230 ng / g body weight; Figure S3). Treated
473 animals were placed in the swim tunnel (5 L; Loligo systems, Denmark) to recover and
474 acclimated at a low water flow speed (4.5 cm/sec) for 7 min. After, fish were given the U_{crit} test,
475 subjecting the animals to time intervals of a certain flow velocity (increments of 4.5 cm/sec in
476 5 min steps) until the fish could not swim against the water current (fatigued; Figure S3).
477 Fatigue was determined when fish stopped swimming and was forced against the rear net of the
478 tunnel for more than 5 sec. Critical speed was then calculated using the following equation
479 (Brett, 1964):

480

481 $U_{crit} = U_{fatigue} + [U_{step} \times (t_{fatigue} / t_{step})]$,

482

483 *Where:* $U_{fatigue}$ = the highest flow velocity where fish swam the whole interval, U_{step} = velocity
484 increment, $t_{fatigue}$ = time elapsed at final velocity that fish swam in the last interval, t_{step} = time
485 increment that is the duration of one interval. The critical speed was normalized to body length
486 (BL) of the experimental animals and is given as BL/sec.

487

488 For the open field test, treated animals were placed in small dishes (diameter: 8 cm) and allowed
489 to swim freely, while their swimming was recorded for 4 min. Analysis of 2 min swimming
490 behavior was performed after optimization and implementation of wrMTrck, a freely available
491 ImageJ plugin. The average velocity and maximum velocity was normalized to body length
492 (BL) of the experimental animals and is given as BL/sec.

493

494 **Statistics**

495 The significance of differences between the means in experimental groups and conditions was
496 analyzed using the *One-way* ANOVA followed by *post hoc* Tukey test and the two-tailed
497 Student's *t*-test (paired or unpaired), using Prism (GraphPad Software Inc.) Differences were
498 considered to be significant if $p < 0.05$. Data presented here are given as mean ± SEM.

499 **Acknowledgements**

500 We are grateful to A. El Manira for providing the electrophysiology set-up and the zebrafish
501 lines; and K. Meletis and A. Martin for critical assistance with *in situ* hybridization experiments.
502 We also thank A. El Manira, C. Broberger, M. Carlén, G. Silberberg, and P. Williams for
503 valuable discussion and comments of our manuscript. This work was supported by a grant from
504 the Swedish Research Council (2015-03359 to K.A.), StratNeuro (to K.A.) Swedish Brain
505 Foundation (FO2016-0007 to K.A.) and Längmanska kulturfonden (BA17-0390 to K.A.).

506 **References**

507 Alaburda A, Perrier J-F, Hounsgaard J. 2002. An M-like outward current regulates the
508 excitability of spinal motoneurones in the adult turtle. J. Physiol. (Lond.) **540**:875–881.
509
510 Ampatzis K, Ausborn J, Manira El A. 2013. Pattern of innervation and recruitment of different
511 classes of motoneurons in adult zebrafish. J. Neurosci. **33**: 10875–10886.
512
513 Ampatzis K, Song J, Ausborn J, Manira El A. 2014. Separate microcircuit modules of distinct
514 v2a interneurons and motoneurons control the speed of locomotion. Neuron **83**: 934–943.
515
516 Anadón R, Molist P, Rodríguez-Moldes I, López JM, Quintela I, Cerviño MC, Barja P,
517 González A. 2000. Distribution of choline acetyltransferase immunoreactivity in the brain of
518 an elasmobranch, the lesser spotted dogfish (*Scyliorhinus canicula*). J. Comp. Neurol. **420**:
519 139–170.
520
521 Bagnall MW, McLean DL. 2014. Modular organization of axial microcircuits in zebrafish.
522 Science **343**: 197–200.
523
524 Brett JR. 1964. The respiratory metabolism and swimming performance of young sockeye
525 salmon. J. Fish Res. Board Can. **21**: 1183–1226.
526
527 Brown DA. 2010. Muscarinic acetylcholine receptors (mAChRs) in the nervous system: some
528 functions and mechanisms. J. Mol. Neurosci. **41**: 340–346.
529
530 Chevallier S, Nagy F, Cabelguen J-M. 2006. Cholinergic control of excitability of spinal
531 motoneurones in the salamander. J. Physiol. (Lond.) **570**: 525–540.
532
533 Clemente D, Porteros Á, Weruaga E, Alonso JR, Arenzana FJ, Aijón J, Arévalo R. 2004.
534 Cholinergic elements in the zebrafish central nervous system: Histochemical and
535 immunohistochemical analysis. J. Comp. Neurol. **474**: 75–107.
536

Cullheim S, Kellerth JO, Conradi S. 1977. Evidence for direct synaptic interconnections between cat spinal alpha-motoneurons via the recurrent axon collaterals: a morphological study using intracellular injection of horseradish peroxidase. Brain Res. **132**: 1–10.

Deardorff AS, Romer SH, Sonner PM, Fyffe REW. 2014. Swimming against the tide: investigations of the C-bouton synapse. Front Neural Circuits **8**: 106.

Eccles JC, Fatt P, Koketsu K. 1954. Cholinergic and inhibitory synapses in a pathway from motor-axon collaterals to motoneurones. J. Physiol. (Lond.) **126**: 524–562.

Felder CC. 1995. Muscarinic acetylcholine receptors: signal transduction through multiple effectors. Faseb J. **9**: 619–625.

Finkel E, Etlin A, Cherniak M, Mor Y, Lev-Tov A, Anglister L. 2014. Neuroanatomical basis for cholinergic modulation of locomotor networks by sacral relay neurons with ascending lumbar projections. Journal of Comparative Neurology **522**: 3437–3455.

Gabriel JP, Ausborn J, Ampatzis K, Mahmood R, Eklöf-Ljunggren E, Manira El A. 2011. Principles governing recruitment of motoneurons during swimming in zebrafish. Nature Publishing Group **14**: 93–99.

González, A., López, J.M., Sánchez-Camacho, C., Marín, O., 2002. Localization of choline acetyltransferase (ChAT) immunoreactivity in the brain of a caecilian amphibian, Dermophis mexicanus (Amphibia: Gymnophiona). J. Comp. Neurol. **448**: 249–267. doi:10.1002/cne.10233

Goulding M. 2009. Circuits controlling vertebrate locomotion: moving in a new direction. Nat. Rev. Neurosci. **10**: 507–518.

Grillner S, Jessell TM. 2009. Measured motion: searching for simplicity in spinal locomotor networks. Curr. Opin. Neurobiol. **19**: 572–586.

Grillner SS. 2003. The motor infrastructure: from ion channels to neuronal networks. Nat. Rev. Neurosci. **4**: 573–586.

Hassall CJ, Stanford SC, Burnstock G, Buckley NJ. 1993. Co-expression of four muscarinic receptor genes by the intrinsic neurons of the rat and guinea-pig heart. Neuroscience **56**: 1041–1048.

Herron LR, Miles GB. 2012. Gender-specific perturbations in modulatory inputs to motoneurons in a mouse model of amyotrophic lateral sclerosis. Neuroscience **226**: 313–323.

Höglund AU, Baghdoyan HA. 1997. M2, M3 and M4, but not M1, muscarinic receptor subtypes are present in rat spinal cord. J. Pharmacol. Exp. Ther. **281**: 470–477.

Hornby TG, McDonagh JC, Reinking RM, Stuart DG. 2002. Effects of excitatory modulation on intrinsic properties of turtle motoneurons. J. Neurophysiol. **88**: 86–97.

Hosey MM. 1992. Diversity of structure, signaling and regulation within the family of muscarinic cholinergic receptors. Faseb J. **6**: 845–852.

Huang A, Noga BR, Carr PA, Fedirchuk B, Jordan LM. 2000. Spinal cholinergic neurons activated during locomotion: localization and electrophysiological characterization. J. Neurophysiol. **83**: 3537–3547.

Hulme EC, Birdsall NJ, Buckley NJ. 1990. Muscarinic receptor subtypes. Annu. Rev. Pharmacol. Toxicol. **30**: 633–673.

Ichiyama RM, Broman J, Roy RR, Zhong H, Edgerton VR, Havton LA. 2011. Locomotor training maintains normal inhibitory influence on both alpha- and gamma-motoneurons after neonatal spinal cord transection. Journal of Neuroscience **31**: 26–33.

Ireland MF, Funk GD, Bellingham MC. 2012. Muscarinic acetylcholine receptors enhance neonatal mouse hypoglossal motoneuron excitability in vitro. J. Appl. Physiol. **113**:1024–1039.

Jordan L, McVagh JR, Noga BR, Cabaj AM, Majczyński H, Sławińska U, Provencher J, Leblond H, Rossignol S. 2014. Cholinergic mechanisms in spinal locomotion-potential target for rehabilitation approaches. Front Neural Circuits **8**: 132.

Kiehn O. 2006. Locomotor circuits in the mammalian spinal cord. Annu. Rev. Neurosci. **29**: 279–306.

Kurihara T, Suzuki H, Yanagisawa M, Yoshioka K. 1993. Muscarinic excitatory and inhibitory mechanisms involved in afferent fibre-evoked depolarization of motoneurones in the neonatal rat spinal cord. Br. J. Pharmacol. **110**: 61–70.

Miles GB, Sillar KT. 2011. Neuromodulation of vertebrate locomotor control networks. Physiology (Bethesda) **26**: 393–411.

Miles GB, Hartley R, Todd AJ, Brownstone RM. 2007. Spinal cholinergic interneurons regulate the excitability of motoneurons during locomotion. Proc. Natl. Acad. Sci. U.S.a. **104**: 2448–2453.

Mueller T, Vernier P, Wullimann MF. 2004. The adult central nervous cholinergic system of a neurogenetic model animal, the zebrafish Danio rerio. Brain Res. **1011**: 156–169.

Murakami Y, Matsumoto K, Ohta H, Watanabe H. 1996. Effects of oxotremorine and pilocarpine on striatal acetylcholine release as studied by brain dialysis in anesthetized rats. Gen. Pharmacol. **27**: 833–836.

Palstra AP, Tudorache C, Rovira M, Brittijn SA, Burgerhout E, van den Thillart GEEJM, Spaink HP, Planas JV. 2010. Establishing zebrafish as a novel exercise model: swimming economy, swimming-enhanced growth and muscle growth marker gene expression. PLoS ONE **5**, e14483.

Pullen AH, Athanasiou D. 2009. Increase in presynaptic territory of C-terminals on lumbar motoneurons of G93A SOD1 mice during disease progression. Eur. J. Neurosci. **29**: 551–561.

Quinlan KA, Buchanan JT. 2008. Cellular and synaptic actions of acetylcholine in the lamprey spinal cord. J. Neurophysiol. **100**: 1020–1031. doi:10.1152/jn.01157.2007

638 Satou C, Kimura Y, Higashijima S-I. 2012. Generation of multiple classes of V0 neurons in
639 zebrafish spinal cord: progenitor heterogeneity and temporal control of neuronal diversity.
640 Journal of Neuroscience **32**: 1771–1783.
641
642 Saxena S, Roselli F, Singh K, Leptien K, Julien J-P. Gros-Louis F, Caroni P. 2013.
643 Neuroprotection through excitability and mTOR required in ALS motoneurons to delay disease
644 and extend survival. Neuron **80**: 80–96.
645
646 Skup M, Gajewska-Wozniak O, Grygielewicz P, Mankovskaya T, Czarkowska-Bauch J. 2012.
647 Different effects of spinalization and locomotor training of spinal animals on cholinergic
648 innervation of the soleus and tibialis anterior motoneurons. Eur. J. Neurosci. **36**: 2679–2688.
649
650 Song J, Ampatzis K, Björnfors ER, Manira El A. 2016. Motor neurons control locomotor circuit
651 function retrogradely via gap junctions. Nature **529**: 399–402.
652
653 Stil A, Drapeau P. 2016. Neuronal labeling patterns in the spinal cord of adult transgenic
654 Zebrafish. Dev Neurobiol **76**: 642–660.
655
656 Thiriet G, Kempf J, Ebel A. 1992. Distribution of cholinergic neurons in the chick spinal cord
657 during embryonic development. Comparison of ChAT immunocytochemistry with AChE
658 histochemistry. Int. J. Dev. Neurosci. **10**: 459–466.
659
660 Uemura O, Okada Y, Ando H, Guedj M, Higashijima S-I, Shimazaki T, Chino N, Okano H,
661 Okamoto H. 2005. Comparative functional genomics revealed conservation and diversification
662 of three enhancers of the isl1 gene for motor and sensory neuron-specific expression. Dev. Biol.
663 **278**: 587–606.
664
665 Welton J, Stewart W, Kerr R, Maxwell DJ. 1999. Differential expression of the muscarinic m2
666 acetylcholine receptor by small and large motoneurons of the rat spinal cord. Brain Res. **817**:
667 215–219.
668
669 Wullimann MF, Rupp B, Reichert H. 1996. Neuroanatomy of the zebrafish brain: a topological
670 atlas. Basel: Birkhaeuser Verlag.

671 Zagoraiou L, Akay T, Martin JF, Brownstone RM, Jessell TM, Miles GB. 2009. A cluster of
672 cholinergic premotor interneurons modulates mouse locomotor activity. Neuron **64**: 645–662.
673
674 Zhang H-M, Li D-P, Chen S-R, Pan H-L. 2005. M2, M3, and M4 receptor subtypes contribute
675 to muscarinic potentiation of GABAergic inputs to spinal dorsal horn neurons. J. Pharmacol.
676 Exp. Ther. **313**: 697–704.

Figures

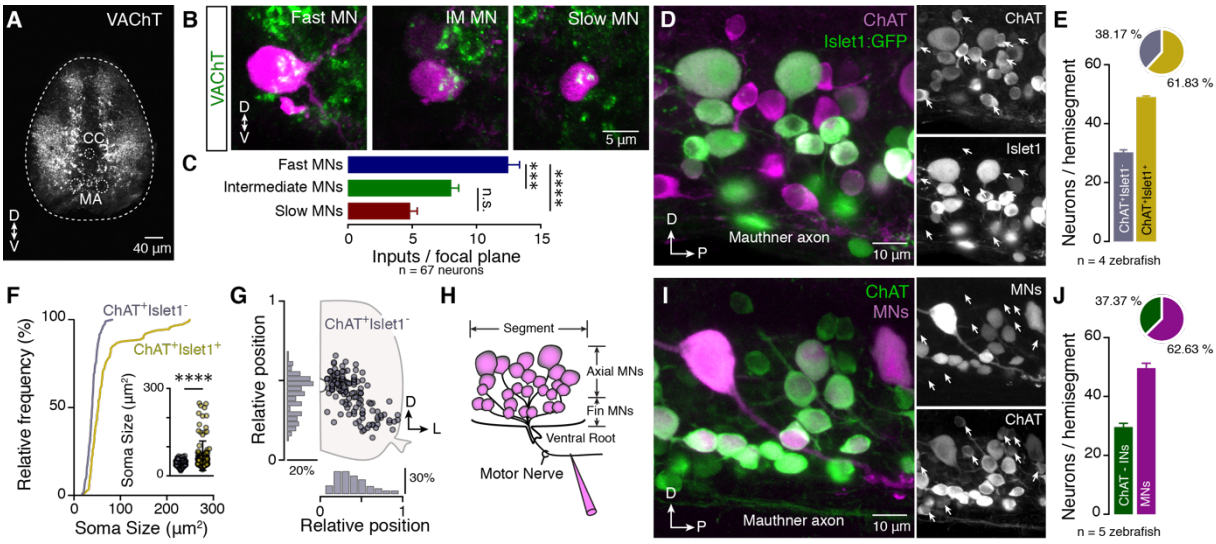

Figure 1. Organization of spinal cholinergic system. (**A**) Distribution of cholinergic terminals within the adult zebrafish spinal cord. (**B**) Single optical sections show the cholinergic synapses onto different types of motoneurons. (**C**) Cholinergic (ACh) input is different between motoneuron (MN) classes, (n_{slow} = 10, n_{interm} = 27, n_{fast} = 30 neurons; n = 5 zebrafish). (**D**) Whole mount spinal cord image shows that cholinergic interneurons ChAT$^+$Islet1$^-$ exist in adult zebrafish. Arrows indicate the ChAT$^+$Islet1$^-$ neurons (Cholinergic interneurons). (**E**) Quantification of the adult zebrafish cholinergic neurons, in *Islet1:GFP* line, per spinal cord hemisegment (n = 4 zebrafish). (**F**) Cholinergic interneurons (ChAT$^+$Islet1$^-$) have smaller soma sizes compared to motoneurons. (**G**) Distribution pattern of cholinergic interneurons (ChAT$^+$Islet1$^-$) within the adult zebrafish spinal cord. (**H**) Drawing showing the methodological approach to backfill all the motoneurons (axial and fin) exiting the spinal cord through the ventral root by injecting a retrograde tracer (Dextran). (**I**) Whole mount spinal cord immunohistochemistry reveals that a fraction of ChAT$^+$ neurons are not backfilled motoneurons. Arrows indicate ChAT$^+$MN$^-$ neurons (Cholinergic interneurons; n = 5 zebrafish). (**J**) Quantification of the adult zebrafish cholinergic neurons, per spinal cord hemisegment (n = 5 zebrafish), reveals similar number of cholinergic interneurons as in the *Islet1:GFP* line. CC, central canal; D, dorsal; L, lateral; MA, Mauthner axon; P, posterior; V, ventral. Data are presented as mean ± SEM; ***p < 0.001; ****p < 0.0001; n.s., non-significant.

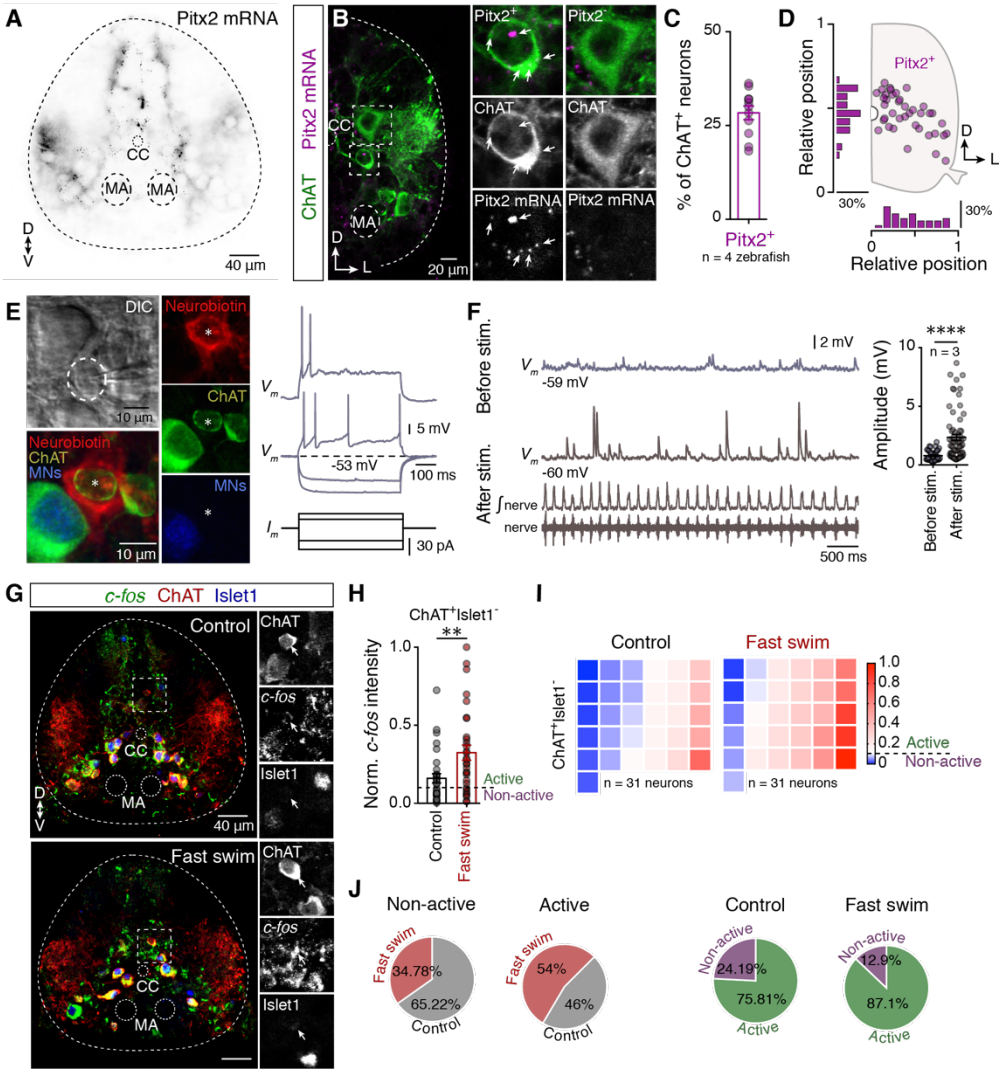

Figure 2. Cholinergic interneurons are homologues to mammalian V0c interneurons and they are recruited at high speed locomotion. (**A**) Localization of *Pitx2 mRNA* in adult zebrafish spinal cord. (**B**) Cholinergic *Pitx2*$^{+}$ and *Pitx2*$^{-}$ neurons found in adult zebrafish spinal cord. Arrows indicate the location of mRNA in the cholinergic neuron. (**C**) Quantification (%) of cholinergic neurons that are *Pitx2*$^{+}$ (n = 4 zebrafish). (**D**) Distribution pattern of cholinergic *Pitx2*$^{+}$ interneurons within the adult zebrafish spinal cord. (**E**) Whole cell patch clamp recording from identified neuron that filled with neurobiotin. Post-hoc evaluation of the patched neuron that is cholinergic (ChAT^{+}) and not motoneuron (MN^{-}). Firing behavior of a representative cholinergic interneuron upon steps of somatic current injections. The asterisk denotes the neurobiotin filled patched neuron. (**F**) Increasing number and amplitude of post-synaptic responses during fictive locomotion, as indicated from the recording of motor nerve activity (lower trace and rectified trace) after electrical stimulation of descending axons to initiate locomotion (n = 3 neurons). (**G**) Microphotographs showing that *c-fos* immunoreactivity increases after prolonged (2h) forced fast swimming (80% of the Ucrit) in the cholinergic interneurons (ChAT^{+}Islet1^{-}). (**H**) Quantification of normalized *c-fos* intensity in cholinergic interneurons (ChAT^{+}Islet1^{-}). The threshold of activity was considered to be 0.11. (**I**) Heat map displaying the normalized *c-fos* intensity of each individual cholinergic interneuron ($n_{control}$ = 31 neurons, $n_{fast\ swim}$ = 31 neurons). (**J**) Proportions of active and non-active cholinergic interneurons (ChAT^{+}Islet1^{-}) between control and after forced fast swimming based on the normalized *c-fos* intensity. CC, central canal; D, dorsal; L, lateral; MA, Mauthner axon; P, posterior; V, ventral. Data are presented as mean ± SEM; **p < 0.01; ****p < 0.0001.

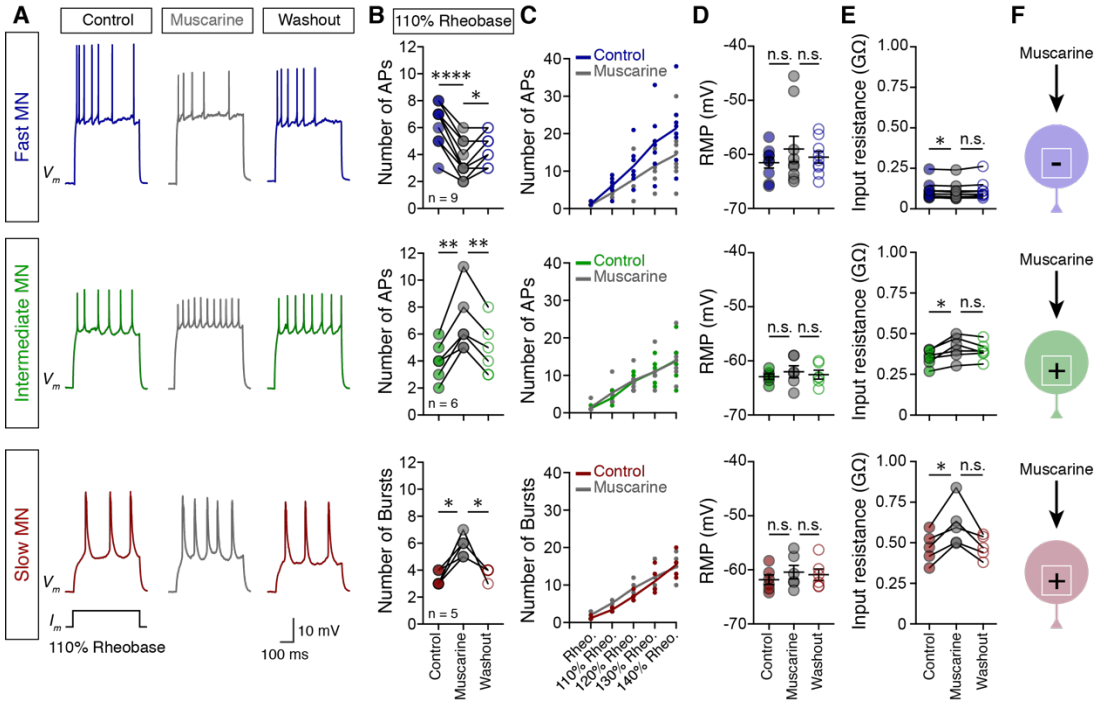

Figure 3. Muscarinic receptors differentially alter motoneuron excitability. (**A**) Representative traces of motoneuron (MN) firing in responses to 110% of rheobase somatic current injection, before (colored traces) after bath application of muscarine (15 μM; gray traces) and followed by washout (colored traces). (**B**) In the presence of muscarine the fast motoneurons significantly reduce the number of action potentials (APs) in response to 110% of rheobase current injection, while both the intermediate and the slow motoneurons increase their firing rate. During washout, the motoneurons partially recover (n_{fast} = 9 neurons, $n_{intermediate}$ = 6 neurons, n_{slow} = 5 neurons). (**C**) Relation of the number of action potentials (APs) or bursts of APs to current (increments of 10% increase from rheobase) in absence (colored line) and presence of muscarine (gray line). (**D**) During the application of muscarine (gray circles) and after washout (open colored circles) there is no significant change in the resting membrane potential of the motoneurons. (**E**) Bath application of muscarine alters the input resistance of all motoneuron types. The input resistance was decreased in the fast motoneurons and increased in the intermediate and slow motoneurons. (**F**) Overview of the change in excitability of different types of MNs in response to muscarine. The sign represents the alteration of the MN excitability (+ = increase, - = decrease). Data are presented as mean ± SEM; *p < 0.05; **p < 0.01; ****p < 0.0001; n.s., non-significant.

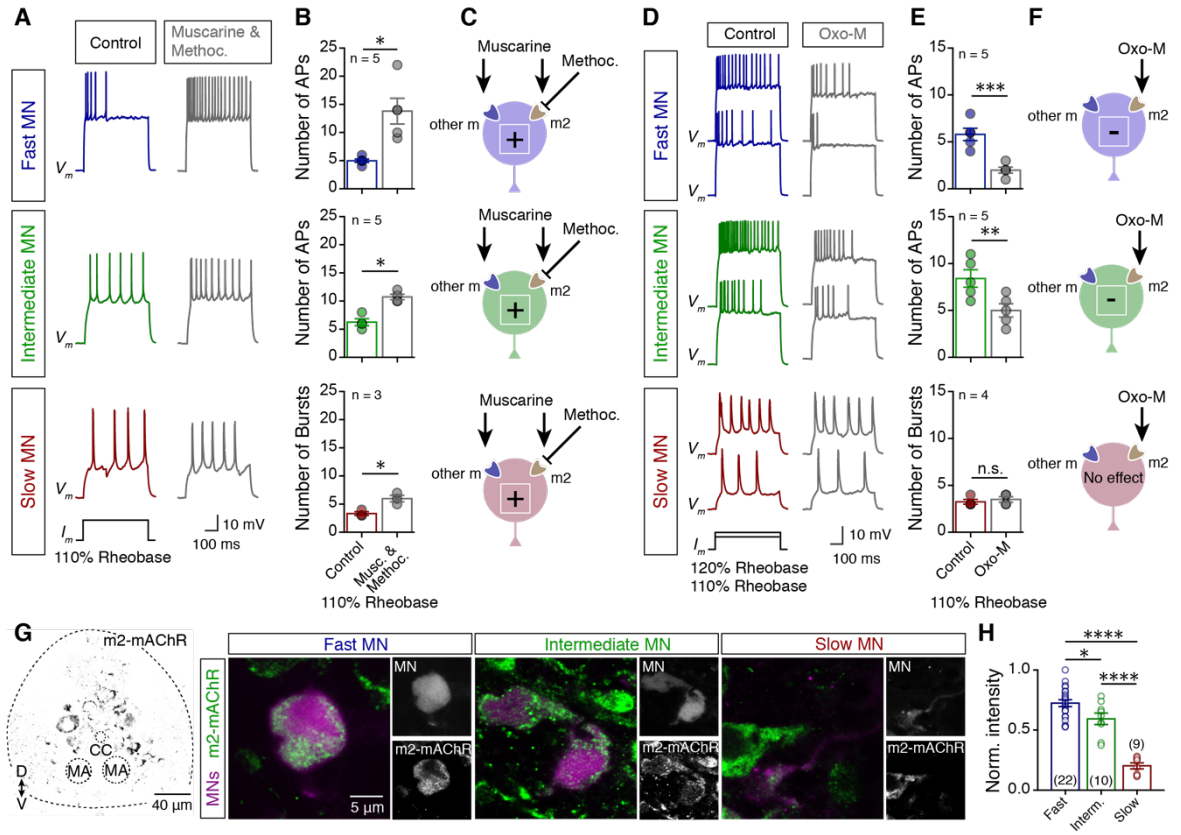

Figure 4. Motoneurons possess different muscarinic receptor subtypes. (**A**) Traces of motoneuron (MN) firing in response to 110% of rheobase current injection, before (colored traces) and after bath application of a mixture of muscarine (15µM) and methoctramine (10µM; gray traces). (**B-C**) Co-application of muscarine and methoctramine produce hyperexcitability in all MN pools (n_{fast} = 5 neurons, $n_{intermediate}$ = 5 neurons, n_{slow} = 3 neurons), derived from the antagonistic effect on m2-mAChRs. (**D**) Representative traces of motoneuron (MN) firing in response to 110% and 120% of rheobase current injections, before (colored traces) and after bath application of oxotremorine-M (Oxo-M; 20 µM; gray traces) which preferentially activates the m2-mAChRs. (**E-F**) In the presence of oxotremorine-M, excitability decreases in the fast and intermediate motoneurons, whereas the slow motoneurons do not change their firing rate in response to 110% of rheobase current injection (n_{fast} = 5 neurons, $n_{intermediate}$ = 5 neurons, n_{slow} = 4 neurons). (**G**) Distribution pattern of m2-mAChRs in relation to different motoneuron types. A combination of retrograde labeling of different motoneuron pools with immunostaining for m2-mAChRs reveals that the fast motoneurons exhibit a vast number of m2 receptors compared to other motoneuron types (intermediate and slow). Slow motoneurons were found to be weakly labeled. The sign represents the excitability alteration of the MN (+ = increase, - = decrease). Data are presented as mean ± SEM; *p < 0.05; **p < 0.01; ***p < 0.001; ****p < 0.0001; n.s., non-significant.

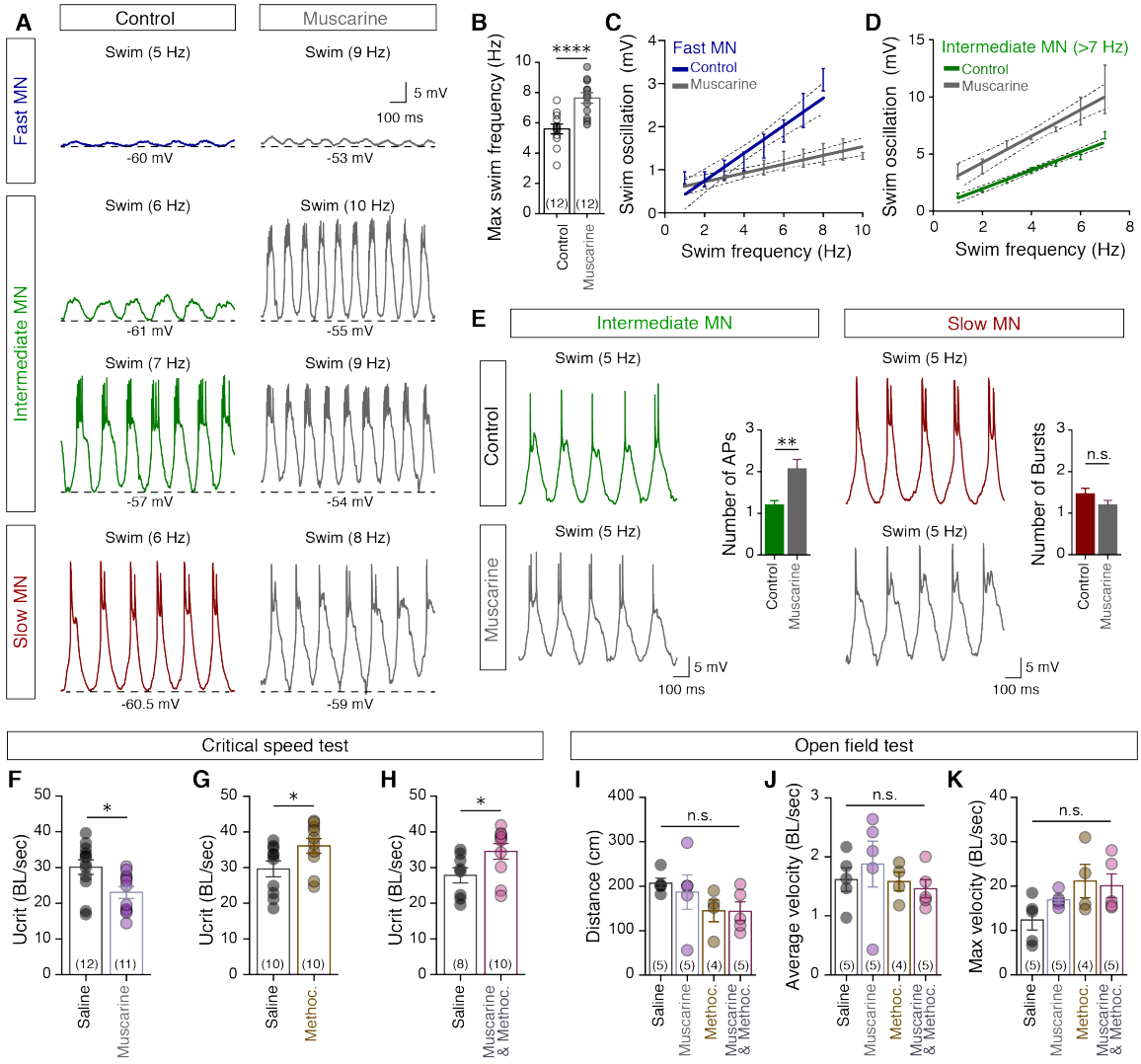

Figure 5. Activation of motoneuron muscarinic receptors controls fast locomotion. (**A-B**) During fictive locomotion, motoneurons display membrane potential oscillations. The highest swimming frequency increases in the presence of muscarine (15 µM; gray traces) during fictive locomotion (*ex vivo* experiments). Dashed line indicates the membrane potential of the lower part of the oscillations. (**C**) Averaged slopes of the membrane potential oscillations in relation to different swimming frequencies of fast motoneurons in the absence (blue line), or presence (gray line) of muscarine. The data are presented as interpolation curve (middle line ± SEM) and 95% confidence band (outer dashed lines).(**D**) Slopes showing the increasing amplitude of the membrane potential oscillations of the intermediate motoneurons recruited above 7 Hz, in relation to the swimming frequency, before and after the application of muscarine. After muscarine (gray line) the amplitude of the membrane oscillations was significant increased ($F = 856.6$ $p < 0.0001$), in comparison to the control (green line). The data are presented as interpolation curve (middle line ± SEM) and 95% confidence band (outer dashed lines). (**E**) During 5 Hz fictive locomotion, in the absence (colored trace) or presence (gray trace) of muscarine, the number of discharges of intermediate motoneurons increased, while slow motoneurons did not display any changes in the number of bursts of action potentials. (**F-H**) Intraperitoneal administration of muscarine reduces the U_{crit} (BL = 1.84 ± 0.11 cm; n = 23 zebrafish), while methoctramine increased the maximum swimming speed (BL = 1.68 ± 0.1 cm; n = 20 zebrafish). Co-administration of muscarine and methoctramine increased the maximum obtained swimming speed (BL = 1.71 ± 0.12 cm; n = 18 zebrafish). (**I-K**) *In vivo* monitoring of adult zebrafish locomotor behavior. Muscarine and/or methoctramine administration was not found to affect the distance traveled, the average velocity and the maximum velocity of the studied animals (n = 19 zebrafish). The data were normalized to body lengths

(BL) / sec. Data are presented as mean ± SEM; *p < 0.05; **p < 0.01; ****p < 0.0001; n.s., non-significant.

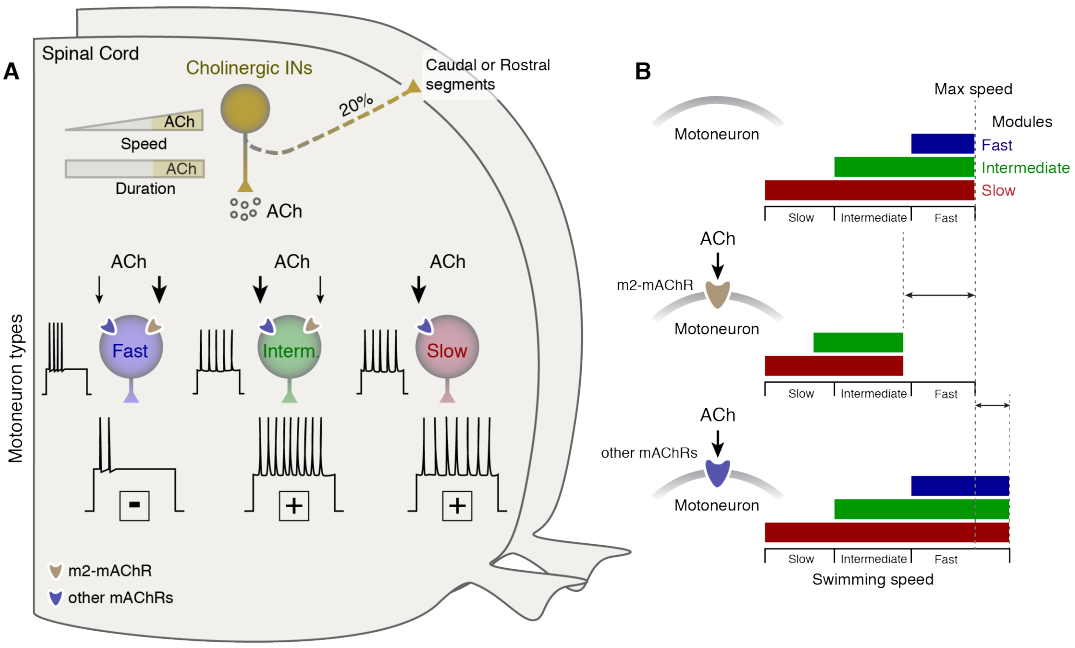

Figure 6. Differential organization of cholinergic input to MNs permits changes of the operational range of locomotor circuit. (**A**) Acetylcholine release (after prolonged fast swimming) from spinal cholinergic interneurons affects the excitability of different types of motoneurons in a mAChR dependent manner. Our results clearly demonstrate that acetylcholine can only increase slow motoneuron excitability, whereas the intermediate and fast motoneurons can alter their excitability through the activation of the different mAChRs that they possess. (**B**) This configuration allows the animals to adjust the recruitment of the locomotor microcircuit modules and alter the operational range of these networks.

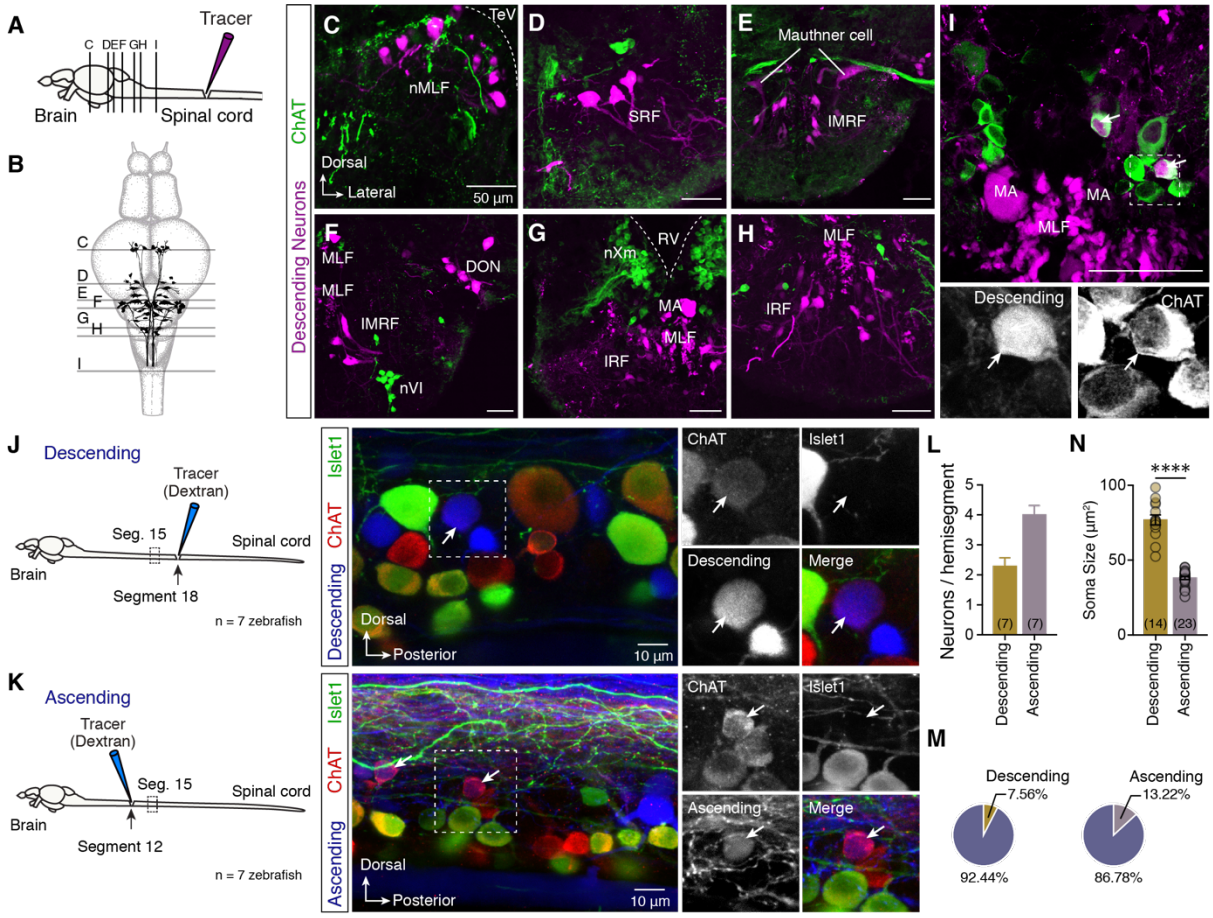

Supplementary file 1. All the brain neurons descending to spinal cord are not cholinergic. (**A-B**) Injection of methylrhodamine dextran in the spinal cord retrogradely labels all the descending supra-spinal neurons (N = 8 zebrafish brains). Schematic representation of the distribution of adult zebrafish brain descending neurons with the level of sections that correspond to the following images in C-I. (**C-H**) Confocal images show that none of the descending labeled neuron is ChAT^{+} in all studied brain areas. (**I**) Few descending neurons (n = 4 neurons out of 8 brains) were found to be ChAT^{+} in the initial part of the spinal cord. Arrows indicate the double labeled neurons. (**J**) Injection of a retrograde dextran tracer in spinal segment 18 reveals the descending interneurons located in spinal cord segment 15. Few descending neurons that are cholinergic (ChAT^{+}) and not motoneurons (Islet1^{-}) were found in the spinal hemisegment of adult zebrafish. Arrow indicates cholinergic descending interneuron. (**K**) Injection of dextran retrograde tracer in spinal segment 12 reveals the ascending interneurons in spinal cord segment 15. Arrows indicate a small number of retrograde traced neurons that are cholinergic interneurons (ChAT^{+} Islet1^{-}). (**L**) Analysis of the number of the cholinergic interneurons that possess a descending (2.28 ± 0.28 neurons / hemisegment; n = 7 zebrafish) or an ascending (4 ± 0.3 neurons / hemisegment; n = 7 zebrafish) axon. (**M**) Percentage of the descending and ascending cholinergic interneurons per hemisegment of spinal cord. (**N**) The descending and ascending cholinergic interneurons have non-overlapping soma sizes ($t = 13.4$, $p < 0.0001$, n = 37 neurons), suggesting that different populations of cholinergic interneurons are ascending or descending in adult zebrafish spinal cord. DON, descending octaval nucleus; IMRF, intermediate reticular formation; IRF, inferior reticular formation; MA, Mauthner axon; MLF, medial longitudinal fascicle; nMLF, nucleus of the medial longitudinal fascicle; nVI, abducens nucleus; nXm, vagal motor nucleus; RV, rhombencephalic ventricle; SRF, superior reticular formation; TeV, tectal ventricle. Data are presented as mean ± SEM; ****$p <$ 0.0001.

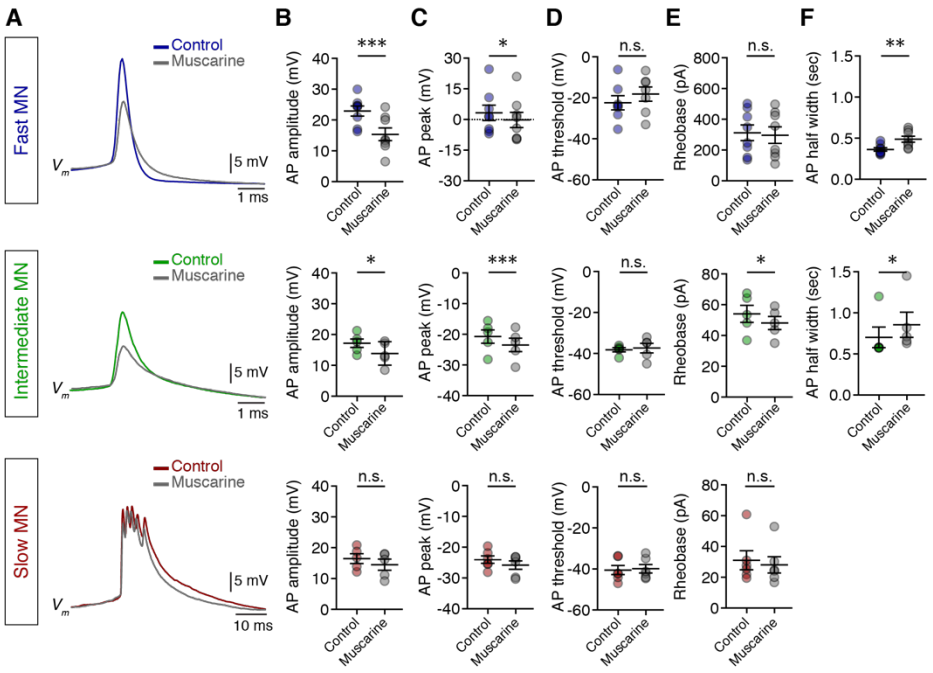

Supplementary file 2. Changes in MN intrinsic biophysical properties after the bath application of muscarine. (**A**) Superimposed representative examples of the first action potential (AP) in fast and intermediate motoneurons and first burst of action potentials (APs) of slow motoneurons before (colored traces) and after (gray traces) muscarine. (**B**) The AP amplitude was significantly reduced by muscarine in intermediate ($t = 4.33$, $p = 0.0123$, $n = 5$) and fast motoneurons ($t = 5.66$, $p = 0.0008$, $n = 8$). (**C**) Following the reduction of AP amplitude also the AP peak was found to be hyperpolarized (Fast MNs: $t = 2.44$, $p = 0.044$, $n = 8$; intermediate MNs: $t = 14.64$, $p = 0.0001$). (**D**) Muscarine application was found not to affect the AP threshold. (**E**) Rheobase, the minimum current injection that generates an AP, was hyperpolarized in intermediate motoneurons ($t = 4.24$, $p = 0.013$, $n = 5$). (**F**) The half-width duration of the AP was significantly increased by muscarine in motoneurons firing single APs (intermediate MNs: $t = 3.79$, $p = 0.019$, $n = 5$; fast-MNs: $t = 4.9$, $p = 0.0017$, $n = 8$). Student's paired t test. Data are presented as mean ± SEM; *$p < 0.05$; **$p < 0.01$; ***$p < 0.001$; n.s., non-significant.

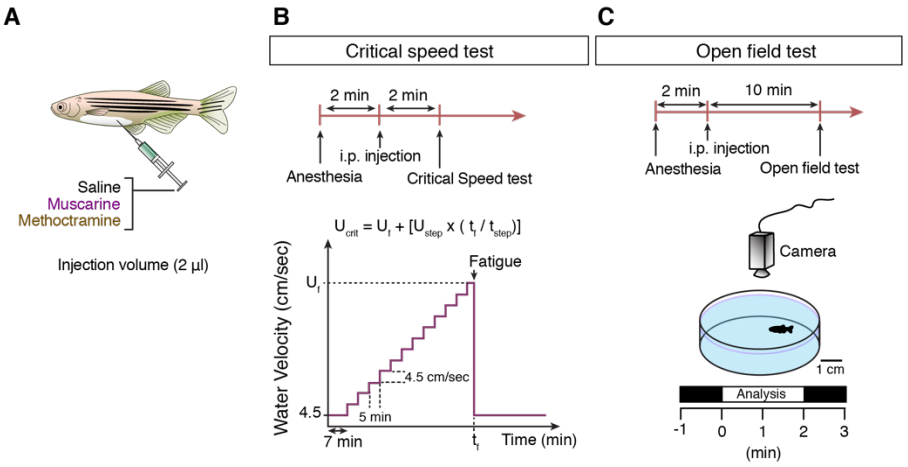

Supplementary file 3. Experimental design to investigate the effect of mAChRs during *in vivo* locomotion. (**A**) Intraperitoneal administration of saline, muscarine and/or methoctramine in anesthetized adult zebrafish before the *in vivo* tests. (**B**) The critical speed test protocol. (**C**) Protocol for *in vivo* monitoring of adult zebrafish locomotor behavior.